Title

Transport Resistances in Fuel-Cell Catalyst Layers

Journal

ECS Transactions, 80(8)

ISSN

1938-5862

ISBN

978-1-62332-477-3

Authors

Chowdhury, Anamika

Radke, Clayton J

Weber, Adam Z

Publication Date

2017-08-24

DOI

10.1149/08008.0321ecst

Peer reviewed

ECS Transactions, 80 (8) 321-333 (2017)
10.1149/08008.0321ecst ©The Electrochemical Society

Transport Resistances in Fuel-Cell Catalyst Layers

A. Chowdhury[a,b], C. J. Radke[a], and A. Z. Weber[b]

[a] Chemical and Biomolecular Engineering Department, University of California, Berkeley, California 94720, USA
[b] Energy Technologies Area, Lawrence Berkeley National Lab, Berkeley, California 94720, USA

Mass-transport resistances observed with low platinum (Pt) loadings in polymer-electrolyte fuel-cell (PEFC) catalyst layers (CLs) limit performance and thus, present challenges for necessary further Pt reduction to enable commercialization. It is believed that this resistance is due to mass-transport resistance near the Pt surface, probably due to transport through the ionomer thin-film layer on the Pt/C particles; the nature and genesis of this resistance needs to be explored further. In this study, a hydrogen-pump configuration operated at limiting-current is used to study local mass-transport limitations in CLs. Using an agglomerate model, analytical expressions for the total resistance at limiting current are developed to identify critical parameters controlling this resistance. The dependence of CL resistance on these parameters is examined.

Introduction

Polymer-electrolyte fuel cells (PEFCs) are emerging as a promising alternate energy source with applications in several sectors such as transportation. However, the need for Pt catalyst makes them prohibitively expensive, thereby preventing large-scale commercialization. Further, large mass-transport resistances are observed while operating low-Pt loading catalyst layers (CLs) at high current densities. This resistance sets a lower limit of the amount of Pt loading required in PEFCs.

Recently, several studies have indicated the presence of a local mass-transport resistance close to the Pt site. Greszler et. al. (1) performed oxygen limiting-current experiments to demonstrate that the total CL resistance scales linearly with the inverse of the roughness factor (roughness factor equals the electrochemically active area normalized by the CL geometric area). This resistance was not influenced by operating pressure and could not be explained by bulk-ionomer properties.

Weber et. al. (2) examined the local mass-transport resistance from an ionomer perspective, explaining that the resistance perhaps originates from the ionomer thin-film and becomes dominant at lower Pt-loading CLs due to higher flux per Pt particle for the same current as compared to higher Pt-loading CLs. The structure of the ionomer thin-film is believed to be different from bulk ionomer membrane due to confinement and specific substrate interactions (3). Ionomer thin-films reported lower water uptake and slower water diffusion. Due to confinement, the ionomer adopts more of an aligned lamellar morphology compared to the more

isotropic one in bulk ionomer (4). Since the water domains play a critical role in proton and gas transport, confinement effects can cause low gas transport rates through the ionomer thin film.

Another common hypothesis is that the increased mass-transport resistance is due to Pt/sulfonate group interactions. The sulfonate groups in ionomer chains can adsorb on a Pt surface and reduce the effective Pt area available for current generation. Fushinobu et. al. (5) observed an increase in local resistance with increasing concentration of sulfonate groups. Litster et. al (6) investigated transport resistance through ionomer thin-film (~50 nm) on polycarbonate mesh substrates with no platinum. They did not observe any increased resistance and the overall transport could be explained by bulk diffusional properties. While there is evidence supporting both the school of thoughts, much remains to be explored to conclusively determine the cause of high local resistances in CLs.

In this study, we use a hydrogen-pump configuration operating at limiting-current to explore the mass-transport resistances. As described by Spingler et. al. (7), this configuration helps eliminate other resistances allowing us to probe the mass-transport resistance alone. The goal is to model the CL resistance using the spherical agglomerate structure for limiting current case and examine parameters influencing the CL resistance.

Theory: Spherical Agglomerate Analytical Model

Agglomerate models for the CL allow inclusion of microscopic details in a macrohomogeneous model and are commonly used for PEFC simulations. The model assumes the presence of spherical agglomerates of Pt/Carbon catalyst particles covered by ionomer thin-films. Here, we incorporate the CL agglomerate model in a 1-D analytical model.

A differential cell with high flowrate at the counter electrode (CE) and very low reactant concentration at the working electrode (WE) was used for experiments as shown in Fig. 1. The transport resistance across the flow channels and resistances at the counter electrode are assumed negligible. The average reactant concentration, C_0, in the flow channels can be calculated based on feed hydrogen concentration, inlet hydrogen mass flowrate, and hydrogen mass consumption rate as described by Spingler et. al (7). The two-component Stefan-Maxwell diffusion equations reduce to Fick's law for dilute species and are employed here. The gas from the flow fields diffuses to the CL through the gas-diffusion layer (GDL). The local, steady-state interstitial concentration profile as a function of position can be described by

In GDL for $-l < x < 0$,

$$\frac{d^2 C_{GDL}}{dx^2} = 0 \qquad [1]$$

In CL for $0 < x < L$

$$\frac{d^2 C_{CL}}{dx^2} - \frac{j(x)}{D_{CL} n F \phi_{CL}} = 0 \qquad [2]$$

where C_{GDL} and C_{CL} are the local interstitial concentrations, D_{GDL} and D_{CL} are the effective mass diffusion coefficients in the GDL and CL, respectively, $j(x)$ is the local current volumetric

density, ϕ is the porosity (pore volume per unit volume), F is Faraday's constant, and n is the number of electrons transferred (2). The associated boundary conditions are

$$C_{GDL}\,(x = -l) = C_0$$

$$C_{GDL}\,(x=0) = C_{CL}\,(x=0)$$

$$\frac{dC_{CL}}{dx}\,(x = L) = 0$$

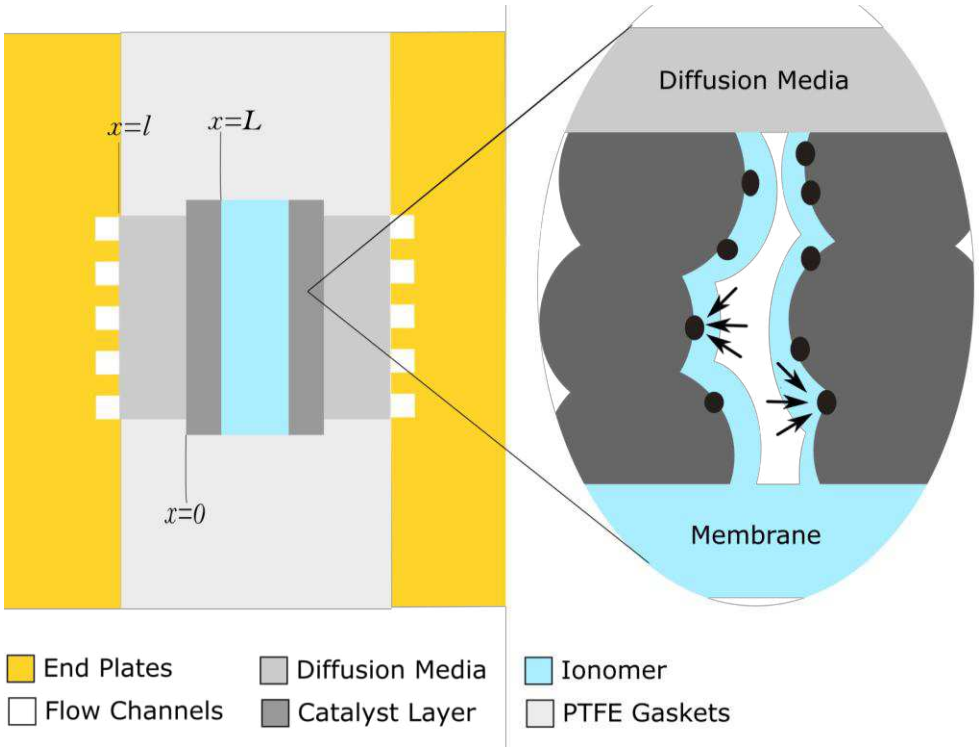

Figure 1. Differential cell schematic used for experiments. The electrode area was controlled by the diffusion media (GDL). The blow-out represents the localized reactant gas diffusion through ionomer thin-films close to Pt particles in CL.

We now use the agglomerate model to evaluate for j in Eqn [2]. The CL is modeled using spherical Pt/C catalyst agglomerates, represented by an effective or average agglomerate diameter. Imaging studies have confirmed that the ionomer is nonuniformly distributed over the agglomerates. Thus, each agglomerate generates a different current.

To evaluate these currents, consider a discrete system where the ionomer thickness δ can take m different values between d_1 and d_2. Let the number of agglomerates with ionomer thickness δ_j per unit volume be represented by n_j and the current from each such agglomerate be represented by I_{δ_j} and can be expressed by

$$I_{\delta_j} = \frac{a * P(T, RH..) * C(x)}{\delta_j}\, nF \qquad [3]$$

where *a* is the active mass transfer area per agglomerate, *P* is the ionomer permeability, which can be a function of several parameters including *d*, and *C(x)* is the local reactant concentration. One must note here that *a* is the active mass transfer area in the limiting-current scenario, where only the Pt particles on the external surface with minimum mass-transfer resistance are active. Since in limiting-current configuration the reaction rate is much higher than the mass-transfer rate, the reactant penetration depth will be minimal and most reactant reacts on or near the surface.

The total current per unit volume *j(x)*, which is the sum of the currents from such individual agglomerate, can be written as

$$j(x) = \sum_{j=1}^{m} n_j I_j \qquad [4]$$

$$j(x) = a_v \sum_{j=1}^{m} n_j \frac{a\, P(T, RH..)\, C(x)}{\delta_j a_v}\, nF \qquad [5]$$

where a_v is the active mass-transfer area per unit volume and is constant for a given membrane-electrode assembly (MEA). The ratio $\frac{a\, n_j}{a_v}$ represents the fraction of active area covered by ionomer thickness δ_j

Let the distribution of ionomer thickness versus % carbon surface area to be represented by *f* such that $f(\delta_j)$ represents the fraction of carbon surface covered by ionomer thickness δ_j. Assuming the total active area to be uniformly distributed across each agglomerate, $f(\delta_j)$ then also represent the ratio $\frac{a\, n_j}{a_v}$. Thus, equation [5] simplifies to

$$j(x) = a_v \sum_{j=1}^{m} f(\delta_j) \frac{P(T, RH..)\, C(x)}{\delta_j}\, nF \qquad [6]$$

The continuous analog for the system, with ionomer thickness continuously varying between d_1 and d_2, is

$$j(x) = a_v \int_{d_1}^{d_2} f(\delta) \frac{P(T, RH..)\, C(x)}{\delta}\, nF d\delta \qquad [7]$$

We now make further assumptions to simplify equation [7]. First, we assume that the ionomer thin-film permeability is only a function of temperature and humidity and does not vary with ionomer thickness within the range d_1 *to* d_2. Second, we refer to the experimental imaging data presented by Weber et. al. (8) to approximate $f(\delta_j)$ using a combination of uniform and normal distribution. Further details are presented in the Appendix.

Based on these assumptions and substituting for $f(\delta)$, Eqn [7] simplifies to

$$\frac{j}{nF} = a_v P C(x)\left[\frac{\theta}{d' - d_1}\log\left(\frac{d'}{d_1}\right) + \int_{d'}^{d_2}\frac{1-\theta}{\sqrt{2\pi\sigma^2}\delta}\exp\left(-\frac{(\delta-\mu)^2}{2\sigma^2}\right)d\delta\right] \quad [8]$$

where d_1-d' is the range for uniform distribution, d'-d_2 is the range for normal distribution, μ and σ are the mean and standard deviation of normal distribution, respectively, and θ is the fraction of carbon surface following uniform distribution for ionomer thickness. The integral term in Eqn [8] is approximated using series expansion (see Appendix) to a non-dimensional finite constant C. Equation [8] can be written as

$$\frac{j}{nF} = a_v P C(x)\left[\frac{\theta}{d' - d_1}\log\left(\frac{d'}{d_1}\right) + \frac{(1-\theta)C}{\sqrt{2\pi\sigma^2}}\right] = \frac{a_v P C(x)}{\delta_{eff}} \quad [9]$$

Substitution of Eqn [9] into Eqn [2] gives the following expression for limiting-current density

$$C_{CL}(x) = \frac{C_0\cosh(\alpha(L-x))}{\left[\cosh(\alpha L) + \frac{l\alpha D_{CL}}{D_{GDL}}\sinh(\alpha L)\right]} \quad [10]$$

$$i = -D_{CL}\frac{dC_{CL}}{dx}(x=0) = \frac{C_0 nF}{\frac{1}{\alpha D_{CL}\tanh(\alpha L)} + \frac{l}{D_{GDL}}} \quad [11]$$

where $\alpha = \sqrt{\frac{Pa_v}{\delta_{eff} D_{CL}\Phi_{CL}}}$

In Eqn [11], the denominator represents the total resistance, with the first term in the denominator being the resistance caused by the CL and the second term being that caused by the GDL.

If an additional interfacial resistance is incorporated close to the Pt surface, either at the gas/ionomer or ionomer/Pt interface, then the expression for a single particle changes to

$$I_\delta = -\frac{a C(x)}{\left(\frac{\delta}{P} + R_i\right)} nF \quad [12]$$

where $R_i \equiv interfacial\ resistance$. Thus, a similar expression for current density is obtained as in Eqn [11].

As shown in the Appendix, the expected value of αL is less than 0.5. Within this range, we can safely say that tanh(αL) ~ αL. Thus, the current density can be expressed as

$$i = \frac{C_0 nF}{\frac{1}{\alpha^2 L D_{CL}} + \frac{l}{D_{GDL}}} = \frac{C_0 nF}{\frac{\delta_{eff}\Phi_{CL}}{Pa_v L} + \frac{l}{D_{GDL}}} \quad [13]$$

$$R_{CL} = \frac{\delta_{eff}\Phi_{CL}}{P a_v L} \quad [14]$$

Based on the above model, we identify a_vL and δ_{eff} to be critical in determining CL resistance. Since the total Pt loading and ionomer-tocarbon (I/C) ratio by weight are expected to have a direct impact, these parameters are examined in the next section.

Experimental Setup

The experiments were performed using the same setup as described by Spingler et. al. (7) using a ~1 cm^2 cell with 1000 ppm hydrogen diluted in Argon at the WE and 2% hydrogen diluted in Argon at the CE. The CLs were fabricated from ionomer dispersion (Dupont™ DE2020CS) and Pt/HSC particles and were supported on Nafion® NRE212 membrane. The CL thickness was in the range of 4 to 14 micrometers. The WE loading was varied while the CE was maintained at a constant loading of 0.4 mg/cm^2. GDLs used for both electrodes was Sigracet™ 25BC of thickness 235 micrometers.

Characterization of a_v and δ_{eff}

Specific active area a_v

As mentioned previously, only the Pt particles on the external surface of the agglomerate are active at limiting current. Based on the geometric arguments outlined in the Appendix, a_vL is linearly proportional to the total Pt loading. Hence, $R_{CL} \propto {}^{1}/_{ECSA}$, where ECSA is the electrochemically active surface area per unit geometric area (assuming ECSA also is proportional to the total Pt loading, which is confirmed by experimental measurements reported in Appendix Table 1). This dependence has been previously reported by Greszler et. al. (1) using oxygen-limiting current. The experiment was repeated for hydrogen/deuterium limiting current and the results are shown in Fig. 2. Roughness factor denoted by *f* is the inverse of ECSA. The total ECSA was measured using CO stripping method (9). MEA details used for the experiments are provided in the Appendix Table 1. The slope of the curve is defined as the local transport resistance that exists close to the Pt surface. The local transport resistance majorly contributes to the CL resistance. Other constant resistances such as ohmic and contact resistances and mass-transport resistance through the GDL, etc. are included in the intercept of the plot. The local resistance obtained is based on total ECSA. However, if one were to consider only the effective active area being utilized, which is less than the total ECSA, the local resistance, i.e, slope obtained, would be different.

The ratio of deuterium to hydrogen slopes is ~1.3. If the local resistance was purely diffusional in nature, the expected ratio of the slopes would be ~1.4 $\left(\sqrt{{}^{M_{D_2}}/_{M_{H_2}}}\right)$. However, this is not observed thus indicating that the local resistance is not completely diffusional in nature and might include an interfacial resistance as described in previous section.

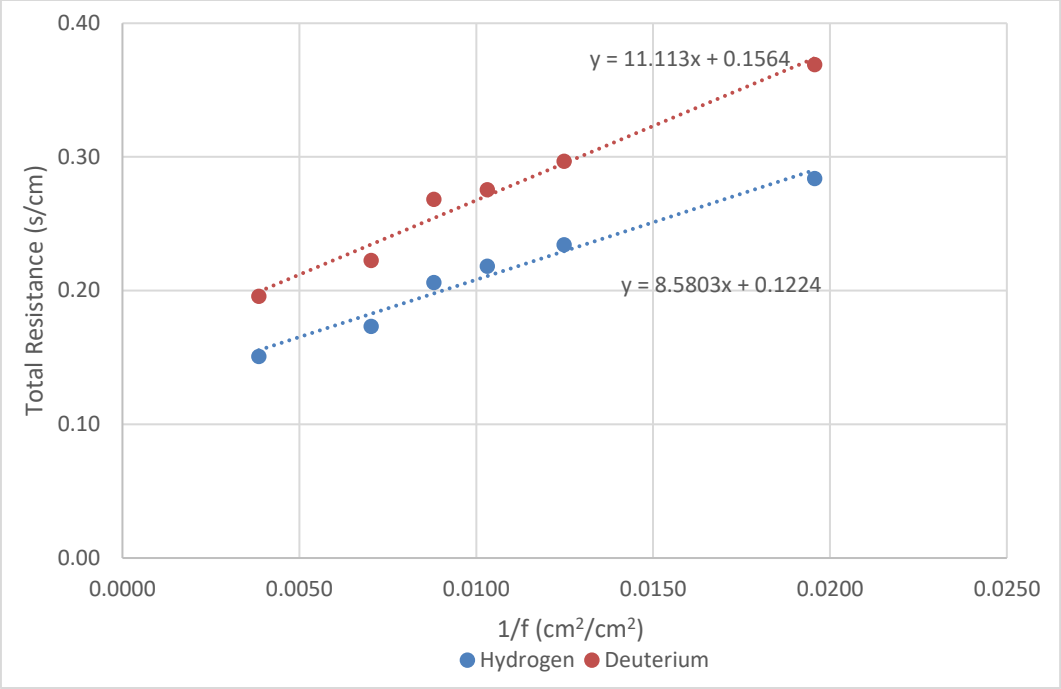

Figure 2. Plot of total resistance vs. I/roughness factor. The WE loading was varied between 0.05mg/cm^2 to 0.4mg/cm2. T= 80C; RH = 80%; Pressure = ambient.

To investigate the impact of I/C ratio on a_v, the ECSA of sample with the constant Pt loading on WE (0.08 mg/cm^2) and varying I/C ratio between 0.6 and 1.1 was measured. The average ECSA for the samples was 83.45 cm^2/cm^2 with a standard deviation of 4.2%, thereby indicating no significant impact of I/C ratio on ECSA.

Thin-film ionomer thickness δ_{eff}

The ionomer thickness in the CL cannot be easily measured unlike ECSA. Among the several parameters that influence I/C, the I/C ratio likely has most significant impact in determining δ_{eff}. We explore the impact of I/C ratio by measuring the total resistance for MEAs with same loading but varying I/C ratio through increasing the ionomer content. Other resistances in the system are assumed constant. Any change in total measured resistance is attributed to the impact of I/C.

Since the additional ionomer in MEAs with higher I/C ratio is not increasing the ECSA, as mentioned in previous section, it may either be depositing as a thicker film on the agglomerates or forming more/larger ionomer pockets or both. Based on limiting-current resistance measurements of MEAs with different I/C ratios and same Pt loading, the total resistance and diffusional resistance with square-root mass dependence is observed to increase linearly with I/C, thereby implying thicker ionomer films, as shown in Fig. 3.

Fig.3 (a) plots the total resistance as a function of I/C ratio. Assuming ohmic and contact resistances are negligible, the intercept gives the sum of GDL and non-mass dependent CL resistance while the slope represents the resistance contributed by ionomer thin-film. The ratio of the slope for deuterium to hydrogen is ~ 1.35, indicating diffusional nature of this resistance.

The total resistance was corrected for the GDL resistance as shown in Fig. 3 (b) (see Appendix for GDL resistance correction), thus giving only the CL resistance.

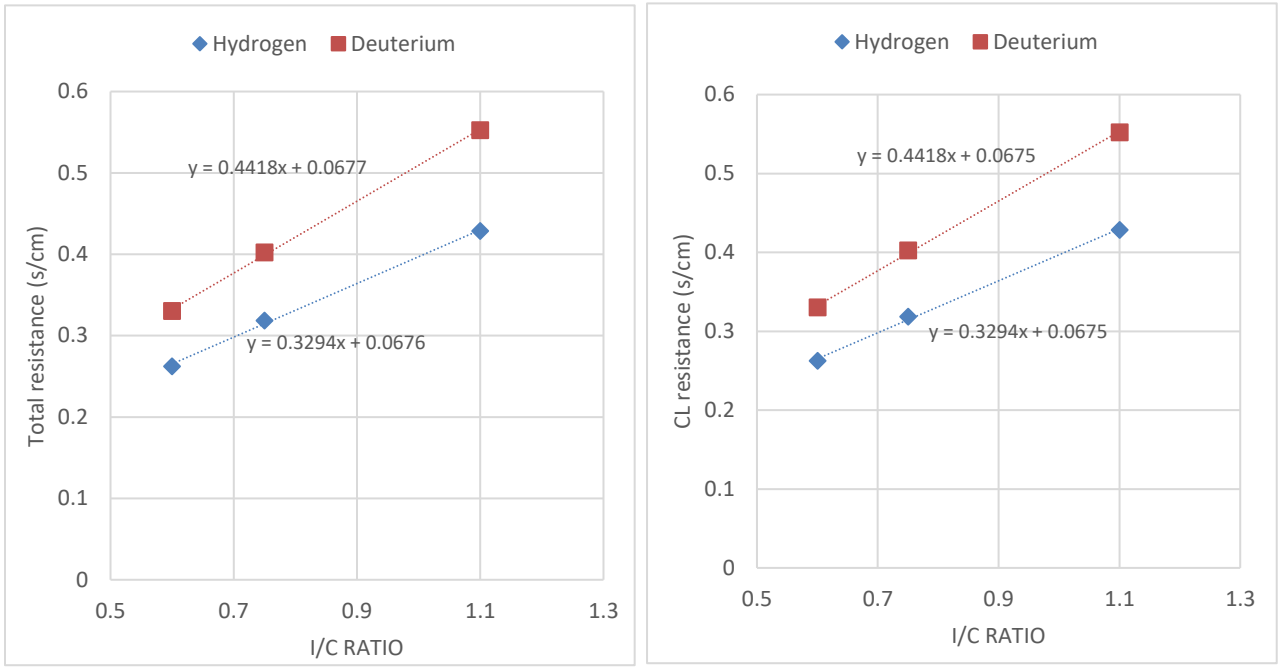

Figure 3. (a) Total Resistance as a function of I/C. The difference in intercepts is due to diffusional resistance. (b) CL resistance obtained from the total resistance corrected for GDL resistance. WE Loading = 0.08mg/cm^2.

The CL resistance can be divided into two parts: (i) diffusional resistance through the ionomer given by the slope and (ii) a mass-independent interfacial resistance represented by the intercept ~ 6.68 s/m. The mass-independent interfacial resistance contributed about 20 to 35% of the total resistance (for I/C of 1.1 to 0.6, respectively) for the MEAs examined. This resistance is thought to be indicative of the sulfonate moiety poisoning on the Pt or perhaps a very dense layer adjacent to the Pt.

However, the above analysis does not rule out the possibility of ionomer pocket formation with increasing I/C, which might also occur simultaneously and needs to be confirmed via imaging studies. In addition, the impact of I/C ratio on CL resistance undoubtedly depends on carbon type, MEA fabrication method, etc. and needs to be explored further.

Summary

In this work, we examined the catalyst-layer (CL) local mass-transport resistance. On incorporating the agglomerate model in the 1-D analytical model for a CL, we identified the active mass-transport area per unit geometric area, a_vL, and effective ionomer thickness, δ_{eff}, as critical in determining the total CL resistance. These properties were examined as a function of I/C ratio. a_vL can be argued to be proportional to the total ECSA and hence would follow the same trends as ECSA. No significant impact of I/C ratio on ECSA was observed, indicating that the additional ionomer added to the CL does not lead to greater carbon surface coverage. The

total and local CL resistance increases linearly with I/C, thereby indicating thicker ionomer films at higher I/Cs. Based on the plot of CL resistance vs I/C, the CL resistance was divided into two parts, first being the diffusional resistance from the ionomer thin-film and second was the mass-independent interfacial resistance, which contributed 20 to 35% of the total CL resistance for the MEAs examined.

Acknowledgements

We would like to thank helpful discussions and data provided by KC Neyerlin at NREL. This work was funded under the Fuel Cell Performance and Durability Consortium (FC PAD) funded by the Energy Efficiency and Renewable Energy, Fuel Cell Technologies Office, of the U. S. Department of Energy under contract number DE-AC02-05CH11231.

References

1. T. A. Greszler, D. Caulk, and P. Sinha, *J. Electrochem. Soc.*, **159**, F831–F840 (2012).
2. A. Z. Weber and A. Kusoglu, *J. Mater. Chem. A*, **2**, 17207–17211 (2014) .
3. K. A. Page, A. Kusoglu, C.M. Stafford, S. Kim, R. J. Kline, and A. Z. Weber, *Nano Lett.*, **14**, 2299–2304 (2014).
4. A. Kusoglu, T. J. Dursch, and A. Z. Weber, *Adv. Funct. Mater.*, **26**, 4961–4975 (2016).
5. Y. Ono, A. Ohma, K. Shinohara, and K. Fushinobu, *J. Electrochem. Soc.*, **160**, F779–F787 (2013).
6. H. Liu, W. K. Epting, and S. Litster, *Langmuir*, **31**, 9853–9858 (2015).
7. F. B. Spingler, A. Phillips, T. Schuler, M. C. Tucker, and A. Z. Weber, *Int. J. Hydrogen Energy*, 1–10 (2017).
8. A. Weber, DOE Fuel Cell Technologies Office Annual Merit Review, (2017) https://www.hydrogen.energy.gov/pdfs/review17/fc137weber 2017_o.pdf.
9. J. Durst, C. Simon, A. Siebel, P. Rheinländer, T. Schuler, M. Hanzlik, J. Herranz, F. Hasché and H. A. Gasteiger, *ECS Trans.*, **64**, 1069–1080 (2014).
10. I. V. Zenyuk, P. K. Das, and A. Z. Weber, *J. Electrochem. Soc.*, **163**, F691–F703 (2016).
11. A. Kusoglu and A. Z. Weber, *Chem. Rev. ACS* (2016).
12. M. Lopez-Haro, L. Guetaz, T. Printemps, A. Morin, S. Escribano, P.-H. Jouneau, P. Bayle-Guillemaud, F. Chandezon, and G. Gebel, *Nat. Commun.*, **5**, 5229 (2014).
13. D. Susac, V. Berejnov, A. P. Hitchcock, and J. Stumper, *ECS Trans.*, **41**, 629–635 (2011).

Appendix

Ionomer thin film distribution

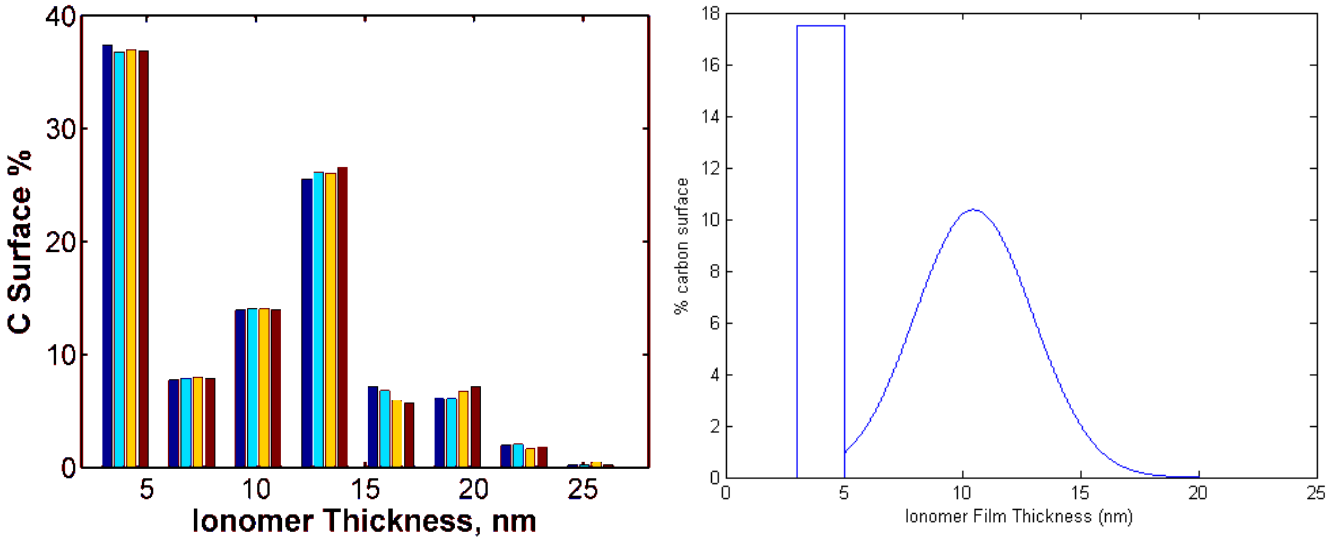

Figure 4. (a) Experimental data for ionomer distribution reported using Nano-CT, TEM, USAXS data (8) (b) Approximation of experimental data as shown in (a) using a combination of uniform distribution and normal distribution.

The function $f(\delta)$ follows a uniform distribution from d_1 to d' and normal distribution from d' to d_2. The distribution is accounted from a minimum value of d_1 since a minimal ionomer thickness is required for proton conduction. Hence, $f(\delta)$ can be represented by the following equations. The mathematical symbols have been defined previously in the text.

$$For\ d_1 < \delta < d' \qquad [15]$$

$$f(\delta) = \frac{\theta}{d' - d_1}$$

$$For\ d' < \delta < d_2 \qquad [16]$$

$$f(\delta) = \frac{1-\theta}{\sqrt{2\pi\sigma^2}} \exp\left(-\frac{(\delta - \mu)^2}{2\sigma^2}\right)$$

Where θ is the fraction of carbon surface following uniform distribution for ionomer thickness between d_1 to d', μ is the mean and σ is the standard deviation

Integrating Ionomer thickness distribution $f(\delta)$

We are interested in calculating the following integral:

$$f(\delta) = \frac{1-\theta}{\sqrt{2\pi\sigma^2}} \exp\left(-\frac{(\delta - \mu)^2}{2\sigma^2}\right) \qquad [17]$$

The exponential term can be expanded using series expansion

$$\exp\left(-\frac{(x-\mu)^2}{2\sigma^2}\right) = \sum_k \frac{1}{k!}\left(-\frac{(x-\mu)^2}{2\sigma^2}\right)^k \quad [18]$$

The absolute value of $\frac{(x-\mu)^2}{2\sigma^2} \sim O(1)$ and scales much slower than *k!*. Hence, we neglect higher order terms (beyond second power). Then, the integral can be written as

$$\int_{d'}^{d_2} \frac{1}{x}\exp(-\frac{(x-\mu)^2}{2\sigma^2})dx = \int_{d'}^{d_2} \frac{dx}{x}\left[1 + \left(-\frac{(x-\mu)^2}{2\sigma^2}\right) + \frac{1}{2!}\left(-\frac{(x-\mu)^2}{2\sigma^2}\right)^2\right] \quad [19]$$

$$\int_{d'}^{d_2} \frac{1}{x}\exp\left(-\frac{(x-\mu)^2}{2\sigma^2}\right)dx = \left[log\left(\frac{d_2}{d'}\right) + \frac{\mu}{\sigma^2}(d_2 - d') + \left(\frac{\mu^2}{4\sigma^4} - \frac{1}{2\sigma^2}\right)(d_2^2 - d'^2) - \frac{\mu}{6\sigma^4}(d_2^3 - d'^3) + \frac{1}{32\sigma^4}(d_2^4 - d'^4)\right]\exp\left(\frac{-\mu^2}{2\sigma^2}\right) = C \quad [20]$$

The resultant of the integral is a finite non-dimensional real number *C*

Calculations for maximum value of αL

$$\alpha = \sqrt{\frac{P a_v}{\delta_{eff} D_{CL} \Phi_{CL}}}$$

We assume the following parameter values:

$D_{CL} = D_{H_2}\frac{\varepsilon}{\zeta}$ = 0.4 cm^2/s (where D_{H_2} is calculated from Chapman-Enskog equation = 4.25cm^2/s and the values of porosity and tortuosity are referred from the studies of Weber et. al. (10)
P = 2.4E-16 mol cm^{-1} s^{-1} Pa^{-1} at 80C, 100% RH (11). In absence of data at 80% RH, this value was used. This value if for bulk ionomer and gives the upper limit on P for calculating maximum value of αL

a_v = This represents the area of Pt particles on the external surface. Based on the highest loading sample used in experiments, ECSA is 32.5E+6 m^{-1}. If we consider agglomerate radius of 50nm (10) and a reactant penetration depth of 5nm (refer to next section for explanation), a_v ~10E+6m^{-1}

δ_{eff} = Here we assume effective ionomer thickness to be ~10nm. Imaging studies usually indicate ionomer thickness between 5-20nm (12)(13). In presence of an interfacial resistance, δ_{eff} will be higher and will further decrease the value of αL

L = ~8μm which is the average CL thickness used in experiments and is also the thickness corresponding to MEA sample with highest loading

Based on above values, max (αL) ~ 0.5

a_v: Linear dependence to total Pt loading

Consider a single agglomerate with total Pt mass loading M_{Pt} and uniform Pt mass density throughout agglomerate volume represented by *D*. This assumption can be made since the agglomerate is made of small individual Pt/Vulcan catalyst particles which have the same Pt loading and the size of individual Pt/Vulcan particles is much smaller than the agglomerate size. Then, the Pt loading on the surface can be defined as

$$m_{Pt}^{surface} = D * 4\pi R^2 dR \quad [21]$$

$$D = {M_{Pt}}/{(4\pi R^3/_3)} \quad [22]$$

$$\frac{m_{Pt}^{surface}}{m_{Pt}^{Total}} = \frac{D4\pi R^2 dR}{D4\pi R^3/_3} = c \quad [23]$$

where R is the agglomerate radius, and dR is the penetration depth enclosing the outer surface Pt particles such that dR << R and dR~R_{PT}, R_{PT} is the radius of one Pt particle. c is the ratio of surface Pt loading to the total loading.

Now if we increase the total Pt mass loading to $(M+dM)_{Pt}$, the above equations change as shown below

$$m_{Pt}^{surface} = D' * 4\pi R^2 dR \quad [24]$$

$$D' = {(M+dM)_{Pt}}/{(4\pi R^3/_3)} \quad [25]$$

$$\frac{m'^{surface}_{Pt}}{m'^{Total}_{Pt}} = \frac{D'4\pi R^2 dR}{D'4\pi R^3/_3} = c \quad [26]$$

Hence, we see that the ratio of surface Pt mass to the total Pt mass remains constant irrespective of the total absolute Pt mass.

Total Resistance vs. $1/f_{Pt}$

Details of MEAs used for experiments are mentioned below. I/C ratio did not have an impact on the thickness of the samples.

WE Loading (mg/cm2)	Catalyst wt%	CL Thickness (µm)	Roughness factor (cm2/cm2)
0.05	20	5	51.12
0.08	20	7.5	80.12
0.10	20	9.3	97.00
0.15	20	14	113.68
0.20	50	4	142.34
0.40	50	8	259.56

GDL Resistance correction

Based on Fig. 3 (a):

H_2 intercept from plot = 0.0676

D_2 intercept from plot = 0.0677

Let intercept resistance = $R_{GDL} + R_{NM}$

where R_{GDL} is the resistance from GDL and R_{NM} is the mass-independent resistance common for both hydrogen and deuterium. Assuming a ratio of 1.38 for $R_{GDL}^{D_2} / R_{GDL}^{H_2}$

$$R_{GDL}^{H_2} + R_{NM} = 0.0676 \quad [27]$$

$$R_{GDL}^{D_2} + R_{NM} = 1.4\, R_{GDL}^{H_2} + R_{NM} = 0.0677 \quad [28]$$

Solving the above two equations, we get $R_{GDL}^{H_2} = 0.0147\,\frac{s}{m}$; $R_{GDL}^{D_2} = 0.0203\,\frac{s}{m}$

The resistances calculated here are order of magnitude lower than the reported literature values (7), possibly due to damage or cracks in the GDL.